Proceedings of IMECE04
2004 ASME International Mechanical Engineering Congress
November 13-20, 2004, Anaheim, California USA

IMECE2004-60700

CRACK TUNNELING: EFFECT OF STRESS CONSTRAINT

Jianzheng Zuo
Department of Mechanical Engineering
University of South Carolina
Columbia, SC 29208, USA

Xiaomin Deng*
Department of Mechanical Engineering
University of South Carolina
Columbia, SC 29208, USA

Michael A. Sutton
Department of Mechanical Engineering
University of South Carolina
Columbia, SC 29208, USA

C.-S. Cheng
GM R&D and Planning
Vehicle Development Research Lab
Warren, MI 48090, USA

ABSTRACT

Crack tunneling is a crack growth feature often seen in stable tearing crack growth tests on specimens made of ductile materials and containing through-thickness cracks with initially straight crack fronts. As a specimen is loaded monotonically, the mid-section of the crack front will advance first, which will be followed by crack growth along the rest of the crack front, leading to the formation of a thumb-nail shaped crack-front profile. From the viewpoint of fracture mechanics, crack tunneling will occur if the operating fracture criterion is met first in the mid-section of the crack front, which may be due to a higher fracture driving force and/or a lower fracture toughness in the mid-section. A proper understanding of this fracture behavior is important to the development of a three-dimensional fracture criterion for general stable tearing crack growth in ductile materials.

In this paper, the phenomenon of crack tunneling during stable tearing crack growth in a single-edge crack specimen is investigated by considering the effect of stress constraint on the fracture toughness. Crack growth in the specimen under nominally Mode I loading conditions is considered. In this case, crack tunneling occurs while the initially flat crack surface (which is normal to the specimen's lateral surfaces) evolves into a final slanted fracture surface. A mixed-mode CTOD fracture criterion and a custom three-dimensional fracture simulation code, CRACK3D, are used to analyze the tunneling and slanting process in the specimen. Results of this investigation suggest that the critical CTOD value (which is the fracture toughness) has a clear dependence on the crack front stress constraint (which is the ratio of the mean stress to the von Mises effective stress). This dependence seems to be linear within the range of stress constraint values found, with the toughness decreasing as the constraint increases. It is found that crack tunneling in this case is mainly the result of a higher stress constraint (hence a lower fracture toughness) in the mid-section of the crack front. Details of the crack growth simulation and other findings of this study will also be presented.

KEYWORDS: crack tunneling, stress constraint, fracture criterion, three-dimensional crack growth simulation

INTRODUCTION

Prediction of ductile fracture in metallic materials has been an important subject of fracture mechanics research. A key focus of this research effort has been the development of fracture criteria for determining the onset and/or direction of crack growth. Currently, several approaches have been proposed to characterize the process of stable crack growth (e.g. J-Integral [1], J-A_2 [2], CTOD [3, 4] or CTOA [5] and so on).

Experimental results (e.g. [6-8]) show that crack tunneling is a common crack growth feature in stable tearing fracture in specimens made of ductile materials. For a specimen containing a through-thickness crack with an initially straight crack front, as the a specimen is loaded monotonically, the mid-section of the crack front will advance first and then the rest of the crack front will grow, leading to the formation of thumb-nail shaped crack-front profiles. In addition to tunneling, slant crack growth may also occur in ductile materials. Stable tearing tests performed on specimens made of AL2024-T3 sheets indicate [6, 7] that slanting occurs when the specimens are in the LT

* Corresponding author; Email: deng@engr.sc.edu

orientation whereas it does not occur when the specimens are in the TL orientation. On the other hand, specimens made of AL 2024-T351 display both flat and slant crack growth in LT orientation [8]. However, what is consistent from these tests is that crack tunneling always occurs regardless of specimen orientation. However, tunneling in flat fracture is usually more severe than that in slant fracture.

From the viewpoint of fracture mechanics, the phenomenon of crack tunneling may be explained using a fracture criterion if a non-uniform fracture driving force and/or a non-uniform fracture toughness exists along the crack front. Specifically, tunneling will occur if the operating fracture criterion is met first in the mid-section of the crack front, either due to a higher fracture driving force and/or a lower fracture toughness in the mid-section. A proper understanding of this fracture behavior is important to the development of a three-dimensional fracture criterion for general stable tearing crack growth in ductile materials.

The present work investigates crack tunneling during stable tearing crack growth in a single-edge crack specimen [6, 7], with a focus on the understanding of the effect of stress constraint on fracture toughness [9, 10], based on a CTOD fracture criterion [3, 4]. It is organized as follows. For reference purposes, Section 2 gives a brief description of the experimental results considered in this study. Section 3 introduces the finite element model and computational approach for simulating crack front evolution observed in the tests. Section 4 presents the distributions of CTOD and stress constraint along different crack fronts based on the simulation results and establishes a correlation between CTOD toughness values and stress constraint values in terms of a linear equation. As an application/verification, this equation is then used in Section 5 as part of the CTOD criterion to enable the simulation of the stable tearing tests to predict crack tunneling profiles during crack growth. The predicted results are compared with experimental measurements. Section 6 presents the conclusions from this study.

CRACK TUNNELING MEASUREMENT

Figure 1 provides a schematic of the single-edge crack specimen geometry [6]. The specimens were machined from rolled 2.3mm-thick sheets made of aluminum alloy 2024-T3. The specimens were then fatigue pre-cracked in the LT orientation so that the initial crack/width ratio, a/w, is 0.0833. To assess the level of crack tunneling, a procedure described in [11] was used to obtain crack front profiles on crack surfaces, which are shown in Figure 2 for stable tearing crack growth in a specimen under remote Mode I loading conditions. The corresponding load for each crack front profile is available from [6].

FINITE ELEMENT MODEL AND COMPUTATIONAL APPROACH

The finite element method is used to analyze the stable tearing crack growth tests described above in order to understand the crack tunneling phenomenon. To carry out such analyses, a finite element code capable of simulating general three-dimensional (3D) crack growth in elastic-plastic solids is required. In this study, the custom code CRACK3D developed at the University of South Carolina is used. Preprocessing (for generating the initial finite element mesh) and postprocessing (for analyzing stress and deformation state at a particular stage of crack growth) are performed using the commercial code ANSYS, through interface options in CRACK3D.

Two simulation options are available in CRACK3D. In the first option (the nodal release option), the crack front is made to advance along a prescribed path, which is accomplished through the release of nodal pairs (the two nodes in a pair are initially tied together by rigid springs) along the crack path when a certain condition (e.g. when a critical load from a test is reached) is satisfied. This option is useful for analyzing fracture tests. In the second option (the local remeshing option), the crack front position is not prescribed but is predicted by a fracture criterion (the CTOD criterion in this study) and a user-specified region around the new crack front is remeshed as the crack front grows.

Figure 3 shows frontal planar views of a 3D finite element mesh used in analyzing the stable tearing tests based on the nodal release option, where Fig. 3(a) is for the entire problem domain and Fig. (b) for a local view of the mesh around the crack front (note that the fatigue crack front has extended from the initial notch into the region on the right). The mesh consists of 8,917 ten-node tetrahedral elements with 14,315 nodes. The minimal element size around the crack front is 0.2 mm. A remote Mode I load was applied in terms of a monotonically increasing displacement, so that nodes at the bottom edge of the specimen were constrained with zero displacements in all directions, and nodes at the specimen's top edge were made to move in the y-direction (vertical direction) (while displacements in the x and z directions were held to zero).

The crack front profiles in the finite element model, which are created based on experimental measurements ([6]), are shown in Fig. 2. Due to slant crack growth, the fracture surface is not flat, hence Fig. 2 is only a projected section view of the actually slant fracture surface (viewed from the positive y-direction; see Fig. 1). The profiles numbered 1, 2, 4, and 6 are for crack fronts measured based on fatigue striation marks during interrupted crack growth tests, and the profiles numbered 3 and 5 are interpolated from profiles 2 and 4, and 4 and 6, respectively. Since the x-y plane coincides with the specimen's mid-plane (where z is zero), the back surface of the specimen corresponds to negative z coordinates and the front surface corresponds to positive z coordinates. A typical 3D crack front profile is shown in Fig. 4.

It is noted that crack front #1 is the initial fatigue crack front and has slight tunneling in the middle. As the specimen is loaded monotonically to the critical load for the onset of crack growth, the middle region of the specimen grows first while the regions near specimen's front and back surfaces remain still. As the load is further increased, the crack front evolves from crack front #1 to #6, with increasing tunneling. The maximum load required for continued crack growth occurred at crack front #6, after which the required load began to decrease gradually.

CRACK3D is used to analyze the tunneling and slanting process in the specimen. With respect to the criterion used during the simulation, the measured critical load corresponding to each crack front is used to control the crack growth at different crack length. The total CTOD (defined as the vector magnitude of its opening, shearing and tearing components) and stress constraint (defined as the ratio of the mean stress to the von Mises effective stress) with regard to the normal plane at each node on crack front are evaluated at the critical instant just before the crack propagation.

In the CTOD criterion [3, 4], the driving force is the total CTOD, which is measured at a fixed distance behind the crack front. In this study, CTOD was strictly computed at a distance of 0.5 mm behind the crack front (along a line normal to the crack front). Since it is impractical to use an extremely refined mesh and an extremely small distance behind the crack front for computing CTOD, and since severe crack tunneling creates a length scale that may not sufficient large compared to 0.5 mm, the computed CTOD is expected to be less accurate in the middle region of a crack front than away from that region. The reason is that, due to severe crack tunneling in the middle region, a point at 0.5 mm (or another small distance) behind the crack front along a line normal to the crack front may be too close to other parts of the crack front, making this point inappropriate for calculating CTOD. To alleviate this problem, it is chosen in the calculation to compute a nominal CTOD value, when the situation noted above occurs, by using the crack-front CTOA value to extrapolate to a distance of 0.5 mm behind the crack front.

It is important to note that, in this analysis phase of the study, crack growth simulations were performed using the nodal release option, with the experimentally measured crack front profile positions and the corresponding loads. The CTOD criterion was not applied even though CTOD variations along the crack fronts were evaluated.

EFFECT OF STRESS CONSTRAINT ON CRITICAL CTOD

The main results of interests from the finite element simulations described in the preceding section are the variations of CTOD and stress constraints along the measured crack fronts, which will be used to establish a correlation between CTOD fracture toughness and stress constraint. Since the CTOD values along a crack front correspond to the critical load that causes growth of the crack front, they are critical CTOD values and equal to the corresponding CTOD fracture toughness values along the crack front.

Figures 5, 6, 7 provide the variations of the total (combined) CTOD and CTOD components for Mode I (opening), Mode II (shearing) and Mode III (tearing) along crack fronts #4, #5, and #6, respectively, at a distance of 0.5 mm behind the crack front (along a line normal to the crack front). In the figures, the through-thickness value refers to the z coordinate value along the crack front. Results for crack fronts in the early stage of crack growth are not shown because these crack fronts have growth only in the middle section and do not provide reliable critical CTOD values (note that CTOD values along parts of the crack front that are not at the impending moment of growth are not critical values and do not equal to CTOD fracture toughness values there).

Two important observations can be made from these figures. First, due to crack tunneling and slanting, a perfect symmetry about the specimen's mid-plane, a feature expected in Model I crack growth, is seen to disappear as crack grows, which lead to a truly three-dimensional mixed-mode CTOD distribution along the crack front, especially in the middle region of the crack fronts. The crack front is Mode I dominant only in the middle region. Second, the total CTOD value (which represents the CTOD-based fracture toughness during crack growth) is not a constant along the crack front—it is lower in the middle region than near the specimen surfaces. As discussed later, this variation in fact reflects the dependence of CTOD toughness on the stress constraint A_m.

Alternatively, variations of the total CTOD along the crack fronts can be plotted in one figure, as shown in Fig. 8. It is seen that the trend shown in the variations along different crack fronts is basically the same. This observation will be utilized subsequently to relate CTOD variation with stress constraint variation along the crack fronts. Before this is done, it must be pointed out that CTOD variations shown so far are strictly computed at a distance of 0.5 mm behind the crack front. Because of severe tunneling (as discussed earlier), the computed CTOD values are less accurate in the middle region of a crack front than away from that region. It is suggested earlier that improved CTOD values in the middle region can be obtained by using the crack-front CTOA value to extrapolate to a distance of 0.5 mm behind the crack front. This seems to be a viable approach for crack fronts after a certain amount of crack growth, so that crack blunting usually seen at the early stage of crack growth can be avoided. Based on this approach, the total CTOD variations in Fig. 8 are updated and are shown in Fig. 9.

Shown in Fig. 10 are the variations of A_m along crack fronts #3, #4, #5, and #6. The constraint value at each crack front point is computed based on an integrated average from the crack front to 0.3 mm ahead of the crack front, in the direction normal to the crack front, within the plane of the crack surface. It must be pointed out that, at and very near the specimen's front and back surfaces, a distance of 0.3mm ahead of a crack front may go outside the specimen domain. In this case, we use the constraint value of the next interior crack front point to approximate the constraint value for the current crack front point. Similar to the total CTOD variations in Fig. 9, a common trend in the stress constraint variations can also be seen.

To reduce scatter in the subsequent data reduction for possible correlation between CTOD toughness and stress constraint A_m, the variations in Figs. 9-10 need to be smoothed. To this end, an averaged total CTOD variation is obtained from Fig. 9 and an averaged stress constraint variation is obtained from Fig. 10. Now, a correlation between CTOD and A_m can be obtained by plotting all (CTOD, A_m) pairs from the same crack front locations, and this correlation is shown in Fig. 11. Clearly, there is a linear correlation between CTOD and A_m, which can be described by the fitted linear equation below (within the range of values for A_m)

$$CTOD=0.0932-0.0312\,A_m \quad (1)$$

Since the CTOD and A_m values are extracted from simulation results of actual fracture tests, with experimentally recorded crack fronts and load values during stable crack growth, there is strong reason to believe that Eq. (1) may represent the dependence of the CTOD based fracture toughness on stress constraint A_m for the material in concern, aluminum alloy 2024-T3. Eq. (1) suggests that the CTOD fracture toughness value is lower when the stress constrain is higher.

If validated by further studies, Eq. (1) can be treated as a material property and will be extremely useful in three-dimensional fracture mechanics applications where constraint effects on fracture toughness are important.

PREDICTION OF CRACK TUNNELING

The relationship between the CTOD toughness and stress constrain can be used to predict crack tunneling based on the CTOD fracture criterion. To demonstrate this application, the Mode I stable tearing fracture test described in previous sections is now simulated. Two types of simulations using CRACK3D are performed.

In the first case, the nodal release option is used with a coarse mesh (to save computation time) with design similar to that in Fig. 3. The mesh consists of 3,308 ten-node tetrahedral elements with 6,169 nodes. The minimal element size around the crack front is 0.4mm. The difference between the simulation here and that in section 4 is that, there are no specified crack front positions on the crack surface except for the initial fatigue crack front (see Fig. 12). The crack front shape is predicted by the CTOD criterion and Eq. (1) even though the crack front is constrained to grow on the measured slant fracture surface. Since the nodal release option is used, the elements are fixed. As a result, some mesh dependence in the predicted crack front positions is expected (see Fig. 13). The dependence can be reduced if finer meshes are used (a coarse mesh is used here). Alternatively, the crack front profile can be smoothed based on predicted crack growth amounts at difference points along the crack front.

In the second case, instead of using a fixed mesh and the nodal release option, the local remeshing option is used so that the mesh in a user-specified region around the current crack front is remeshed each time the crack front is predicted to grow. Again, the CTOD criterion and the relationship between the CTOD toughness and stress constraint are employed to predict the crack front profile although the crack front is still constrained to grow on the measured slant fracture surface.

All simulations are conducted using CRACK3D. In the simulations, the CTOD criterion is evaluated node by node along the current crack front. A crack-front point will advance along the measured slant fracture surface when the CTOD value at that point reaches the critical value defined by the stress constraint A_m ahead of the crack front according to Eq. (1).

The predicted crack front profiles (without smoothing) during stable crack growth are shown in Fig. 13 (with nodal release) and Fig. 14 (with local re-meshing). In order to make the different crack fronts displayed clearly, some of crack fronts in (Fig. 13) are displayed in dotted lines. From both figures it was found that the crack starts to grow at the mid-section of specimen first, and crack tunneling happens as the crack propagates. The shape of crack front is consistent with the measured crack fronts. The depth of crack tunnel on the crack path increases in the early stage of crack growth, and decreases after the crack extension on the surface of specimen is about 1mm, which is consistent with the measured results.

Comparisons of predicted and measured crack tunneling variations during crack growth can be made by the use of a non-dimensional crack tunneling depth parameter, as defined below and in Fig. 15 (a). Let Δa_1 be the amount of crack extension on the specimen's back surface, Δa_2 the amount of crack extension on the specimen's front surface, and Δa_c the amount of crack extension on the mid-plane of the specimen. The average crack extension on the specimen's front and back surfaces is

$$\Delta a_S = \frac{\Delta a_1 + \Delta a_2}{2} \quad (2)$$

Then the non-dimensional crack front tunneling depth, T, is defined as

$$T = \frac{\Delta a_C - \Delta a_S}{B} \quad (3)$$

where B is the thickness of the specimen. Figure 15 (b) shows the variations of T based on crack-front profile measurements and simulation predictions using the nodal release and local re-meshing options of CRACK3D. A good agreement is observed in both cases.

CONCLUSIONS

In this study the crack tunneling phenomenon is investigated by considering stable tearing crack growth in a single-edge crack specimen made of AL 2024-T3. Although the specimen was loaded remotely under Mode I conditions, severe crack tunneling and slant fracture were both present during crack growth. This test was analyzed using a custom three-dimensional crack growth simulation code, CRACK3D.

Results of this study show that the CTOD-based fracture toughness for the ductile material considered is a function of stress constraint at the crack front. Based on the experimentally recorded crack front profiles and the corresponding critical loads, the simulation results suggest that the relationship between the CTOD toughness and the stress constraint, for AL 2024-T3 and within the stress constraint values, seems to be linear, such that a higher stress constraint value would lead to a lower CTOD toughness value.

Based on this study, crack tunneling in the specimen may be interpreted as the result of a lower CTOD toughness (due to higher stress constraint) at the mid-section of the crack front and a higher CTOD toughness (due to lower stress constraint) near the specimen's front and back surfaces. Good comparisons of the predicted and measured crack front profiles seem to

confirm the result of a previous study [10] that stress constraint is a key parameter in ductile failure and fracture criteria.

ACKNOWLEDGMENTS

The authors gratefully acknowledge the financial support from GM, AFRL (Contract No. 00-3210-27-1) and NASA Headquarters (Grant No. NCC5-174).

REFERENCES

[1] Hutchinson, J.W. and Paris, P.C., Stability analysis of J-controlled crack growth, Elastic-plastic fracture, ASTM STP 668, 37-64, 1979.

[2] Chao, Y.J. and Sutton, M.A., On the fracture of solids characterized by one or two parameters: theory and practice, Journal of the Mechanics and Physics of Solids, 42, 269-647, 1994.

[3] Ma, F., Deng, X., Sutton, M. A., and Newman, J. C., Jr., "A CTOD-based mixed-mode fracture criterion," Mixed-Mode Crack Behavior, ASTM STP 1359, 86-110. 1999.

[4] Sutton, M. A., Deng, X., Ma, F., J. C. Newman, Jr., and M. James, "Development and application of a crack tip opening displacement-based mixed mode fracture criterion," International Journal of Solids and Structures 37, 3591-3618, 2000.

[5] Dawicke, D.S. Sutton, M.A., Newman Jr. J.C. and Bigelow, C.A., Measurement and analysis of critical CTOA for an aluminum alloy sheet, NASA TM 109024. Hampton, VA: NASA LangleyResearch Center; 1993.

[6] Boone, M. L., "Characterization of stable tearing in thin sheet of 2024-T3 aluminum alloy under tension-torsion loading conditions," Master Thesis, Department of Mechanical Engineering, University of South Carolina, 1999.

[7] Sutton, M. A., Helm, J. D. and Boone, M. L., Experimental study of crack growth in thin sheet 2024-T3 aluminum under tension-torsion loading. International Journal of Fracture, 109, 285-301, 2001.

[8] James, M.A. and Newman Jr. J.C., The effect of crack tunneling on crack growth: experiments and CTOA analysis. Engineering Fracture Mechanics, 70, 457-468, 2003.

[9] Hancock, J.W. and Mackenzie, A.C., On the mechanisms of ductile failure in high-strength steels subjected to multi-axial stress-states, *J. Mech. Phys. Solids*, **24**, 147-169, 1976.

[10] Zuo, J., Sutton, M.A. and Deng, X., Basic studies of ductile failure processes and implications for fracture prediction, Fatigue & Fracture of Engineering Materials & Structures, 27, 231-243, 2004.

[11] Dawicke, D.S. and Sutton, M.A., CTOA and crack tunneling measurements in thin sheet 2024-T3 aluminum alloy, Exp. Mech. 34, 357-368, 1994.

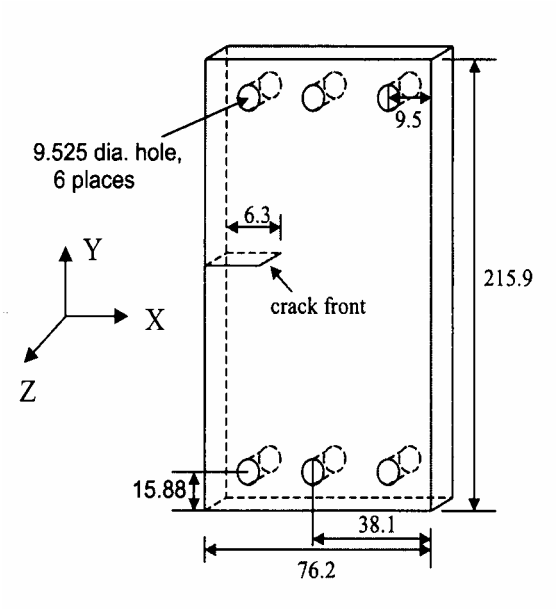

Figure 1 Schematic of a single-edge crack test specimen (all dimensions in mm).

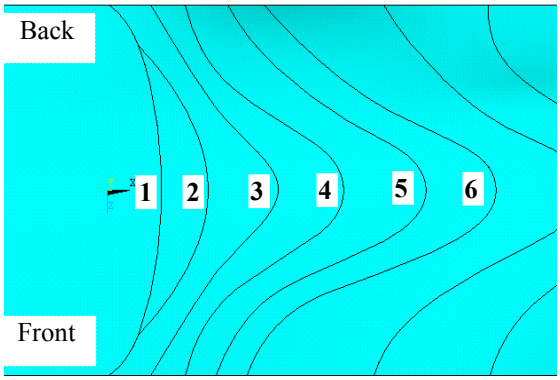

Figure 2 Crack front profiles (after [6]) used in stable tearing crack growth analyses

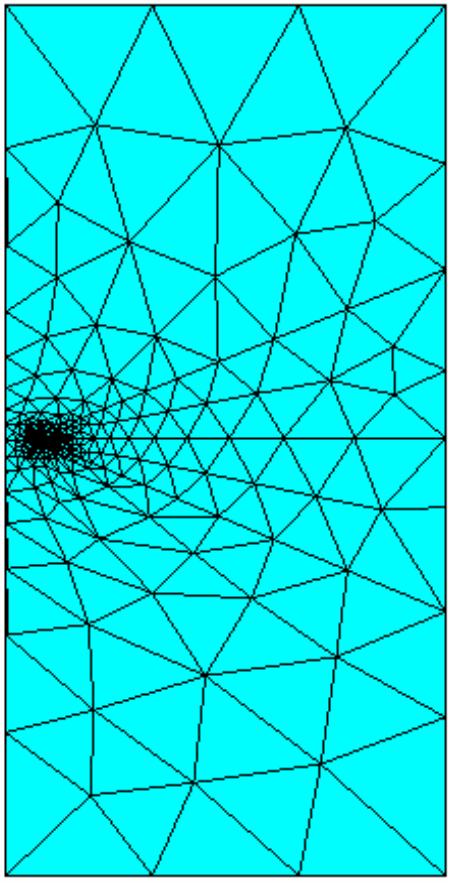

(a)

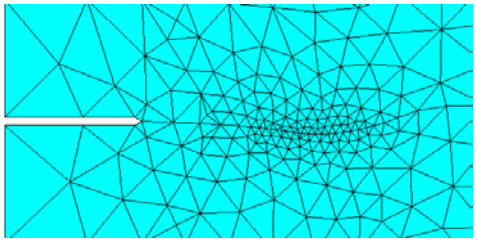

(b)

Figure 3 Frontal views of the finite element mesh: (a) mesh for the entire problem domain and (b) zoomed-in mesh around the crack front.

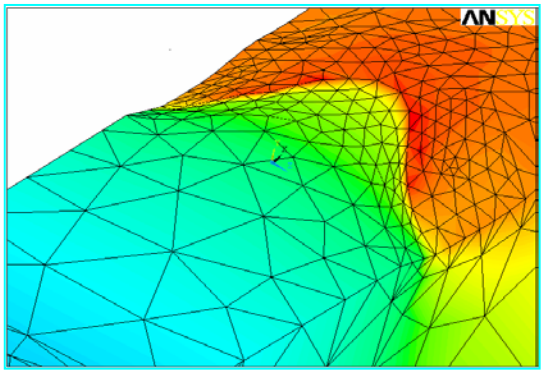

Figure 4 A three-dimensional view of the crack front profile from a stable tearing crack growth test.

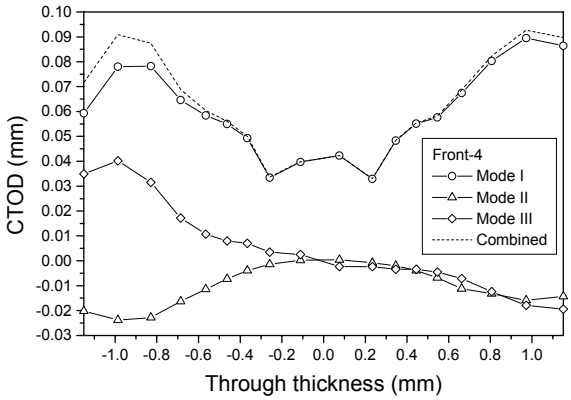

Figure 5 Variation of CTOD and its components along crack front #4.

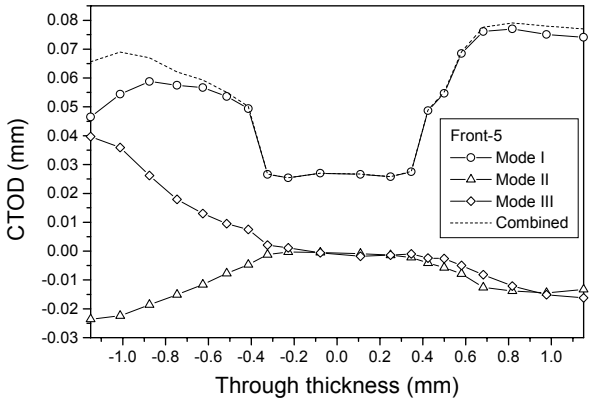

Figure 6 Variation of CTOD and its components along crack front #5.

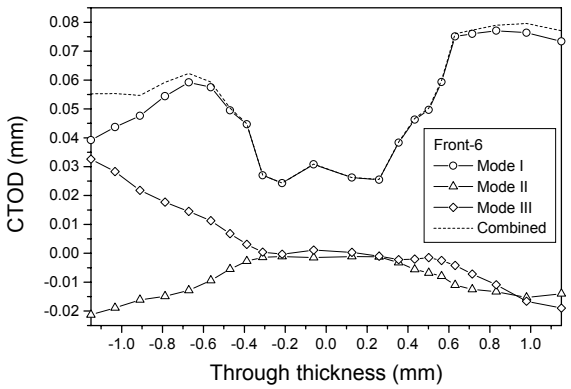

Figure 7 Variation of CTOD and its components along crack front #6.

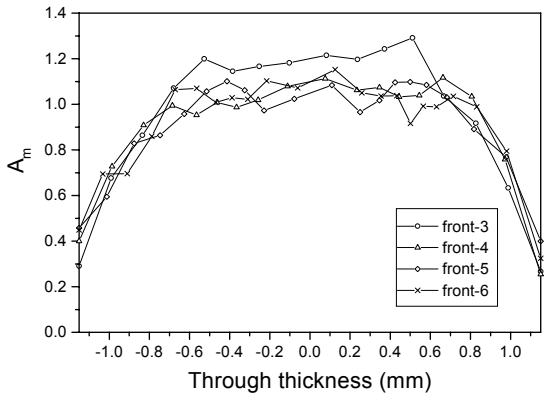

Figure 10 Variation of stress constraint A_m along crack fronts #3, #4, #5, #6.

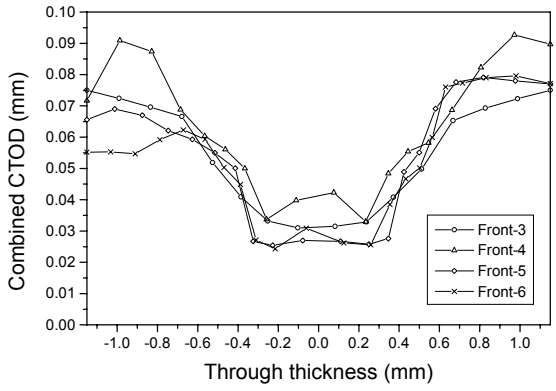

Figure 8 Variation of total CTOD along crack fronts #3, #4, #5, #6 at 0.5 mm behind the crack front.

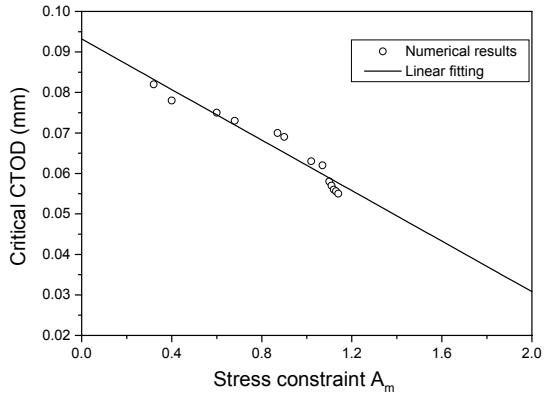

Figure 11 Correlation between the critical CTOD and stress constraint A_m.

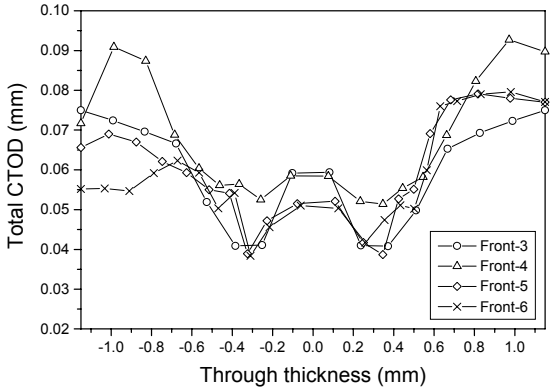

Figure 9 Variation of total CTOD along crack fronts #3, #4, #5, #6 based on improved CTOD calculations in the middle region of the crack front.

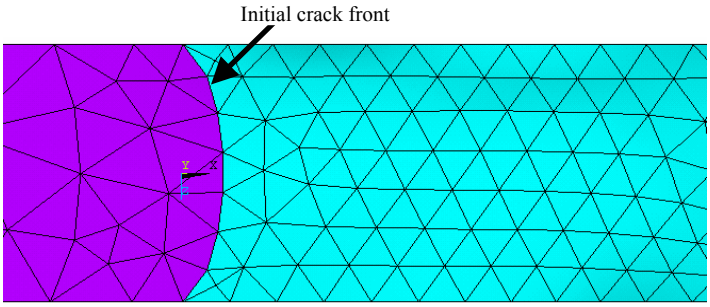

Figure 12 Finite element mesh on the fracture surface.

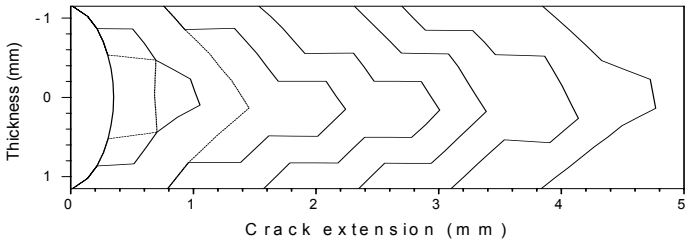

Figure 13 Predicted crack front profiles (with nodal release).

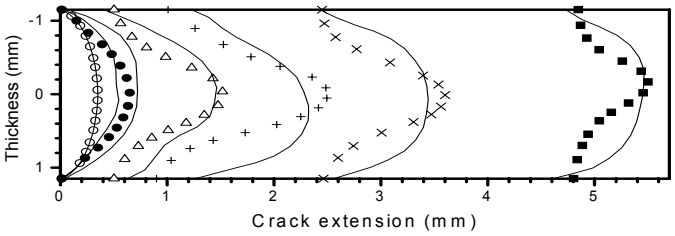

Figure 14 Comparisons of predicted (solid lines, with local re-meshing) and measured (symbols) crack-front profiles.

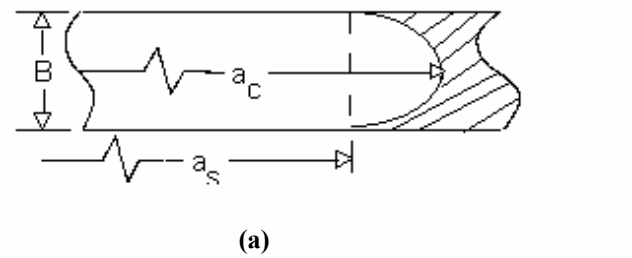

(a)

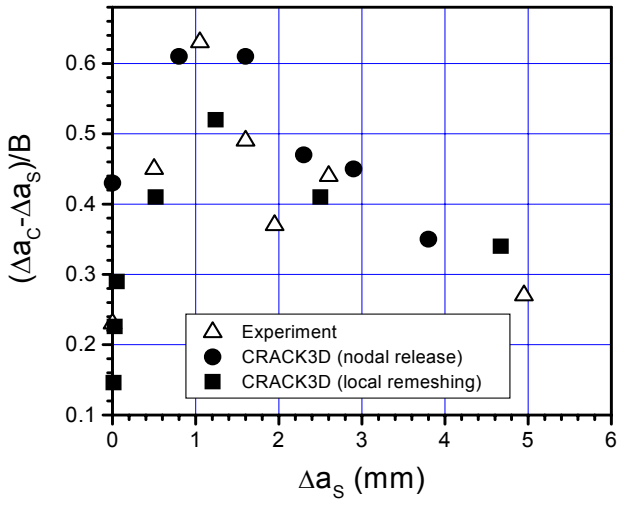

(b)

Figure 15 Crack front tunneling during crack growth: (a) definition of a non-dimensional crack tunneling depth, (b) comparisons of measured and predicted crack tunneling depth variations with crack growth.